Journal of Mines, Metals and Fuels, *71(11): 2143-2149; 2023. DOI: 10.18311/jmmf/2023/36269*

Print ISSN : 0022-2755

Journal of Mines, Metals and Fuels

Contents available at: *www.informaticsjournals.com/index.php/jmmf*

Numerical Simulation of Casson Micropolar Fluid Flow Over an Inclined Surface Through Porous Medium

N. Ramya[1]* and M. Deivanayaki[2]

[1]*Research Scholar, Karpagam Academy of Higher Education, Coimbatore - 641021, Tamil Nadu, India; jpramyamaths@gmail.com.*

[2]*Associate Professor, Department of Science and Humanities, Karpagam Academy of Higher Education, Coimbatore - 641021, Tamil Nadu, India.*

Abstract

Numerical Simulations of Casson Micropolar nanofluid flow over a slanted surface through porous medium is debated in this article. The governing Partial differential equations with various parameters modified to Ordinary differential equations. The set of equations is determined numerically by using MATLAB bvp4c method. The fallout of velocity, Temperature, Concentration and Micro polar on Magnetic, Porous medium profiles is exposed graphically. The implication of Friction drag, Nusselt, and Sherwood numerals for various Magnetic, Casson parameter and Porosity quantities is high lightened in the table.

Keywords: *Chemical Reaction, Micro Polar, Nano Fluid, Numerical Analysis, Porous Medium*

1.0 Introduction

The heat transmission beyond a porous sheet has attracted to its expanding applications in corporation and modern technologies. The MHD flow of mechanized carrying out, insoluble fluid a wide plate that is evenly accelerated and isolated has a precise solution are investigated by Bala Anki Reddy[1]. Nonlinear heat transfer attribute on thermal radiation-influenced magneto hydrodynamic Casson fluid flow in a hall effect are scrutinized by Basavaraj *et al.*, and Deivanayaki *et al.*,[2,3]. The MHD Rayleigh problems with an angled electromagnetic field to determine the impression of a viscous dissipation are studied by Fazle *et al.*,[4]. The heating process and Brownian decay coefficients in the border absorption, the residual of partial slip on the velocity region, as well as turbulent heat barrier case are scrutinized by Hemamalini *et al.*,[5]. The fallout of pedesis diffusion and thermophoretic on dynamically conductive varied flow Casson fluid acquired by a moving wedge are probed by Oyelakin *et al.*,[6]. A arithmetic review on Casson nanofluid horizontal huge surface with a magnetic field effects discussed. The analysis takes into account slip and heat boundary cases are discussed by Imran *et al.*,[7]. The reaction of thermal production and dispersion on MHD in the occupation of heat radiation and synthetic attitude on Casson fluid flow over a perpendicular plate that is oscillating and implanted through porous substances are investigated by Kamran *et al.*,[8]. The Buongiorno nanofluid approach, which are examined the heated performance of the smooth flows under motion of Brownian and thermophoretic phenomena and the operation of nanomaterial are discussed by Hari *et al.*, Anwar *et al* and Venkata Ramudu *et al.*,[9,10,12]. The development of warmth pitch initiation of porous permeability iron deportation on sub heated regular spongy layer is measured by Thomas *et al.*,[11]. The above studies did not take into account of the Numerical findings on casson micropolar nano fluid flow extinct an inclined surface through porous medium. To the best of their understanding, no prior study comprises concepts which are analogous to those in this work.

**Author for correspondence*

The innovation is occupying on the viscous diversion for a non-Newtonian Casson, and the effectiveness of synthetic processes carried on by nanoparticle migrations in the field of producing warmth micropolar nanofluid sample infused in an absorptive medium and exposed to a magnetic field, warmth radiation, and a change in velocity aspect.

2.0 Mathematical Analysis

The subsequent equations for the continuity, momentum, energy and angular momentum

$$\frac{\partial u}{\partial x} + \frac{\partial u}{\partial y} = 0$$

$$u\frac{\partial u}{\partial x} + v\frac{\partial u}{\partial y} = \nu\left(1+\frac{1}{\beta}\right)\left(\frac{\partial^2 u}{\partial y^2}\right) - \left(\frac{k_1}{\rho}\right)\frac{\partial N}{\partial y} + (g\beta_T(T-T_\infty) + g\beta_C(C-C_\infty))\cos\alpha - \frac{\sigma B_0^2 u}{\rho} - \frac{\nu u}{k} \qquad (1)$$

$$u\frac{\partial N}{\partial x} + v\frac{\partial N}{\partial y} = \frac{\gamma}{\rho}\frac{\partial^2 N}{\partial y^2} - \left(\frac{k_1}{\rho}\right)\left(2N + \frac{\partial u}{\partial y}\right) \qquad (2)$$

$$\rho C_p\left(u\frac{\partial T}{\partial x} + v\frac{\partial T}{\partial y}\right) = k\frac{\partial^2 T}{\partial y^2} - \frac{\partial q_r}{\partial y} + q''' + \nu\left(1+\frac{1}{\beta}\right)\rho\left(\frac{\partial u}{\partial y}\right)^2 + \frac{\rho D_m k_T}{C_s}\frac{\partial^2 C}{\partial y^2} \qquad (3)$$

$$u\frac{\partial C}{\partial x} + v\frac{\partial C}{\partial y} = D_m\frac{\partial^2 C}{\partial y^2} - k^*(C - C_\infty) + \frac{D_m k_T}{T_m}\frac{\partial^2 T}{\partial y^2} \qquad (4)$$

The irregular heat parameter is defined by

$$q''' = \frac{k u_w}{x\upsilon}\left(A^*(T_w - T_\infty)f' + B^*(T - T_\infty)\right) \qquad (5)$$

Here A^* and B^* serve heat generation and the internal heat absorption. The warmth discrepancy between T and stream warmth T_∞ is tiny, and by removing components of higher order, Taylor's simplification concerning T_∞ is $T_w = T_\infty + bx$

The equation is the result of using Rosland's similarity for thermal emission,

$$q_r = -\frac{16}{3}\frac{\sigma^*}{k^*}T^3\frac{\partial T}{\partial y} \qquad (6)$$

The confines condition as follows

$$u = u_w + L\frac{\partial u}{\partial y}, -k\frac{\partial T}{\partial y} = h_1(T_\infty - T), -N = -m\frac{\partial u}{\partial y}, D_m\frac{\partial C}{\partial y} = h_2(C_w - C), \quad \text{as } y = 0$$

$$u \to 0, T \to T_\infty, C \to C_\infty \quad \text{as } y = \infty \qquad (7)$$

Where L signifes molecular free mean groove, h_1 and h_2 concentus of deportation and eccentric transmission, C_w liquid's solidification at its outermost layer.

Consider the similarity transforms,

$$\varphi = \sqrt{a\nu}xf(\eta), u = \frac{\partial\varphi}{\partial y} = axf'(\eta), N = ax\left(\sqrt{\frac{a}{\nu}}\right)h(\eta),$$

$$v = -\frac{\partial\varphi}{\partial x} = \sqrt{a\upsilon}f(\eta)$$

$$\theta(\eta) = \frac{T - T_\infty}{T_w - T_\infty}, \qquad \emptyset(\eta) = \frac{C - C_\infty}{C_w - C_\infty},$$

$$T = T_\infty(1 + (\theta_w - 1)\theta) \qquad (8)$$

Using Equation of (8) the equations. (2)–(4) are reconstruct as

$$\left(1+\frac{1}{\beta}\right)f''' + ff'' - (f')^2 + Kh' + (Gr_T\theta + Gr_c\phi)\cos\alpha - (M + k_p)f' = 0 \qquad (9)$$

$$\left(1+\frac{K}{2}\right)h'' + fh' - f'h + K(2h + f'') = 0 \qquad (10)$$

$$[1 + N_r\{1 + 3(\theta_w - 1) + 3(\theta_w - 1)^2\theta^2 + (\theta_w - 1)^3\theta^3\}]\theta'' + N_r[(\theta_w - 1)(\theta')^2 + 6(\theta_w - 1)^2\theta(\theta')^2 + 3(\theta_w - 1)^3\theta^2(\theta')^2] + P_r f\theta' - P_r f'\theta + A^* f' + B^*\theta + P_r Du\phi'' + P_r E_c\left(1+\frac{1}{\beta}\right)(f'')^2 = 0 \qquad (11)$$

$$\phi'' + Scf\phi' - k_r Sc\phi + ScSr\,\theta'' = 0 \qquad (12)$$

Where

$$Gr_T = \frac{g\beta_T(T_w - T_\infty)}{a^2 x}, N_r = \frac{16\sigma^* T_\infty^3}{3kk^*},$$

$$Gr_C = \frac{g\beta_C(C_w - C_\infty)}{a^2 x}, Pr = \frac{\upsilon\rho C_p}{k} = \frac{\mu C_p}{k}, M = \frac{\sigma B_0^2}{a\rho}$$

$$Sr = \frac{D_m K_T}{\upsilon T_m}\left(\frac{T_w - T_\infty}{C_w - C_\infty}\right), Sc = \frac{\upsilon}{D_m},$$

$$\mathrm{Du} = \frac{D_m K_T (C_w - C_\infty)}{C_s C_p \upsilon (T_w - T_\infty)}, E_c = \frac{u^2}{C_p (T_w - T_\infty)}, K_r = \frac{k^*}{a} \tag{13}$$

The changed confines conditions as follows

$f' = 1 + \gamma f'', \ f = 0, \ \theta' = Bi_T(1-\theta), \ \emptyset' = Bi_c(1-\emptyset)$ as

$\eta \to 0,$

$$f'(\eta) = 0, \ \theta(\eta) = 0, \ \emptyset(\eta) = 0 \text{ as } \eta \to \infty \tag{14}$$

The friction drag, Nusselt and Sherwood numeral are the physical confines need attention and defined[12] as follows

$$C_{f_x} Re_x^{\frac{1}{2}} = \left(1 + \frac{1}{\beta}\right) f''(0) \tag{15}$$

$$NuRe_x^{\frac{1}{2}} = -\left(1 + N_r(\theta_w)^3\right)\theta'(0) \tag{16}$$

$$Sh\ Re_x^{-\frac{1}{2}} = -\emptyset'(0) \tag{17}$$

Here, $Re_x = \frac{x u_w}{\upsilon}$ signifies the Reynolds Number.

3.0 Results and Discussion

The nonlinear equations (9) – (14) are disclosed numerically by MATLAB bvp4c method. Consider the numerical values for the graphical results shown below, $\beta = 1.5, Gr_T = 0.8, M = 1.5, Nr = 0.2,$ $A^* = B^* = 0.1, Pr = 7, \theta_w = 2, Gr_c = 0.8,$ $BiT = 2, BiC = 2, Sc = 0.6, Kr = 0.2,$ $Sr = 0.2, Ec = 0.2$ and Du = 0.1. The significance of different deep flow metaphors is demonstrated by friction with the skin visuals, Sherwood and Nusselt computation, and cosmetic regards phases. Figures 1 & 4 display consequences of the magnetic on the micropolar depiction and velocity. A drop in velocity and micro polarity is noticed as soon as the magnetic criterion (M values) is increased. Due to its significant on the movement of fluids, M generates a force as the Lorentz force when imposed through the middle in the preferred direction of flow. Hydrodynamics, plasma accelerators, MHD accelerators, and other technical domains all use the Lorentz force in the electromagnetic force. As consequently, as the magnetic coefficient grows, the

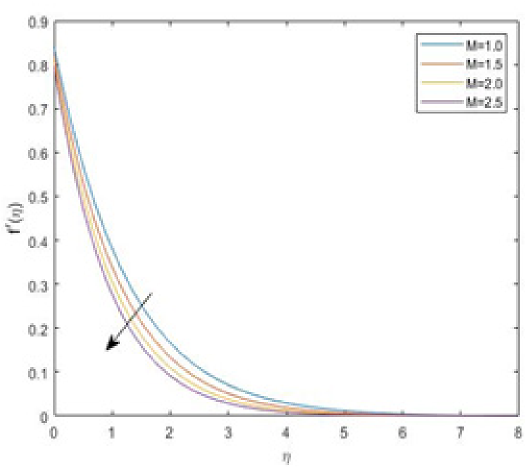

Figure 1. Velocity on diverse of M.

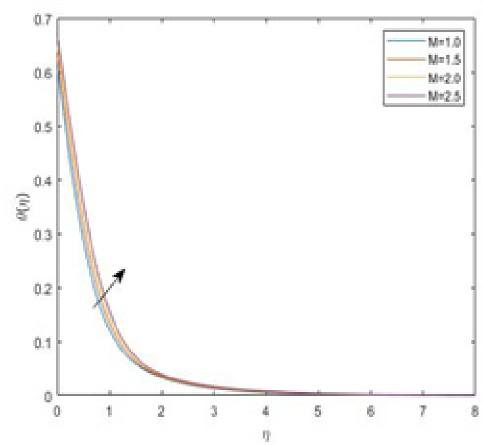

Figure 2. Temperature on diverse of M.

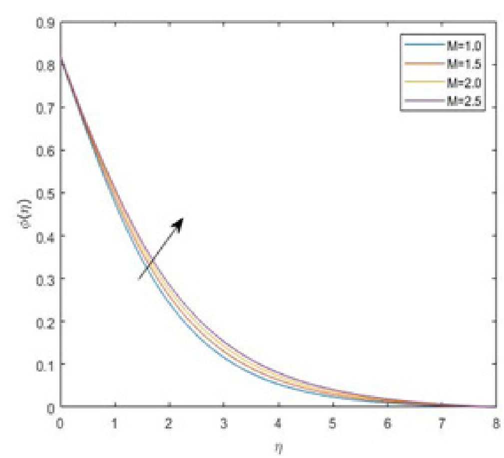

Figure 3. Concentration on diverse of M

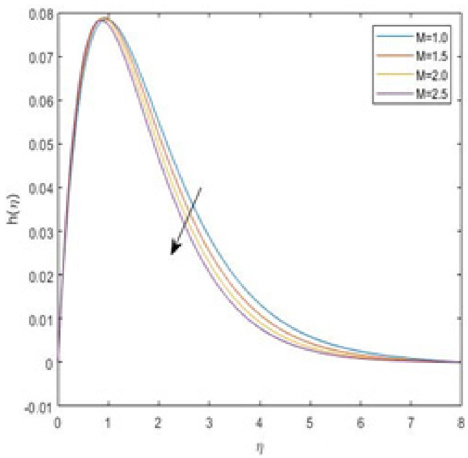

Figure 4. Angular velocity on diverse of M.

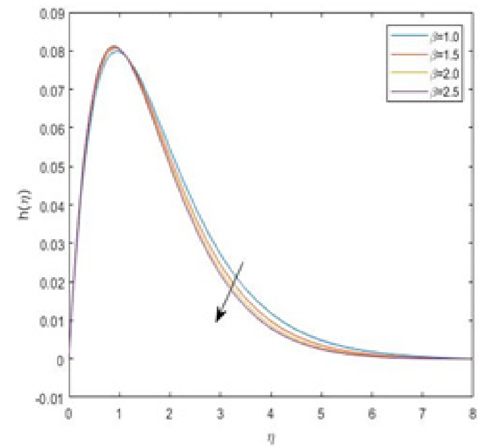

Figure 7. Concentration on diverse of β.

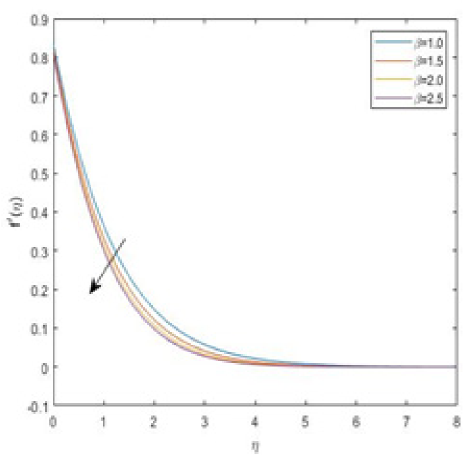

Figure 5. Velocity on diverse of β.

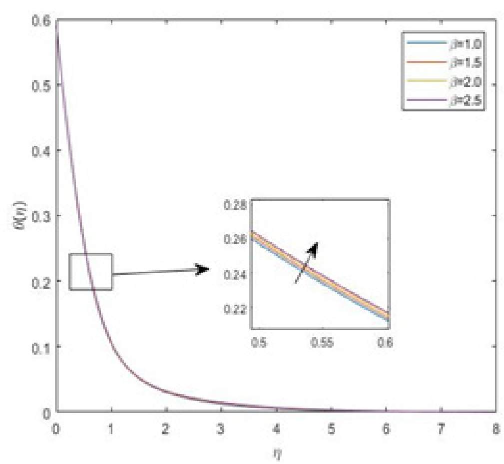

Figure 8. Angular velocity on diverse of β.

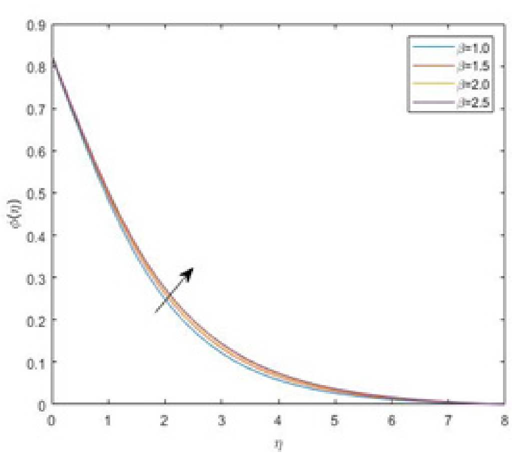

Figure 6. Temperature on diverse of β.

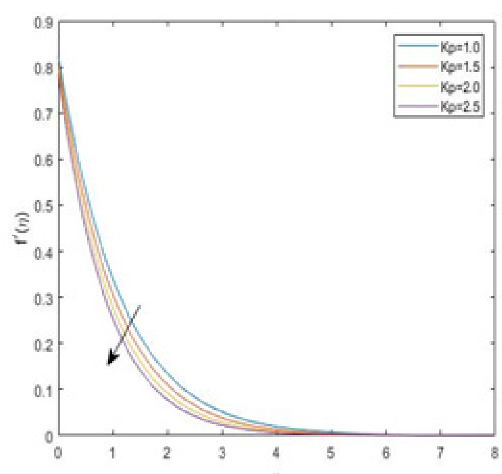

Figure 9. Velocity on *diverse* of K_p

Lorentz force leads the velocity and boundary layer density to decrease. Figures 2 & 3 show when a magnetic parameter grows, the warmth and absorption rise. As the outcome, a force can be created on the tension gradient of the Nano fluid content causing it to subsequently absorb some heat energy.

Figures 5-8 depict Casson parameter on the flow fields momentum, warmth, absorption and micro rotation. Velocity profile and angular velocity declined for larger βwhile θ, ∅ are embellished for the raise β. Figures 9-12 display the velocity profile decrease with increasing porous parameter K_p. The temperature and concentration boosts up for distinct K_p values.

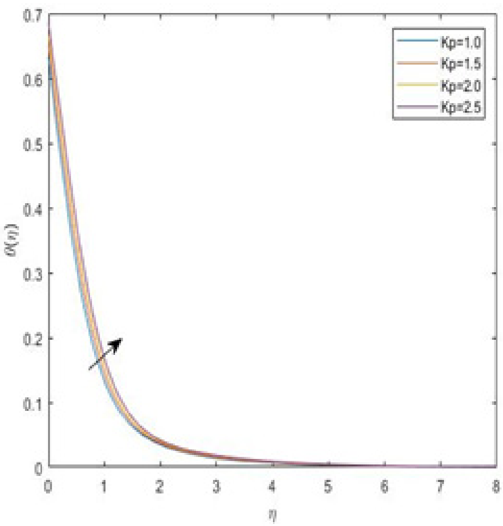

Figure 10. Temperature on *diverse* of $K_{p.}$

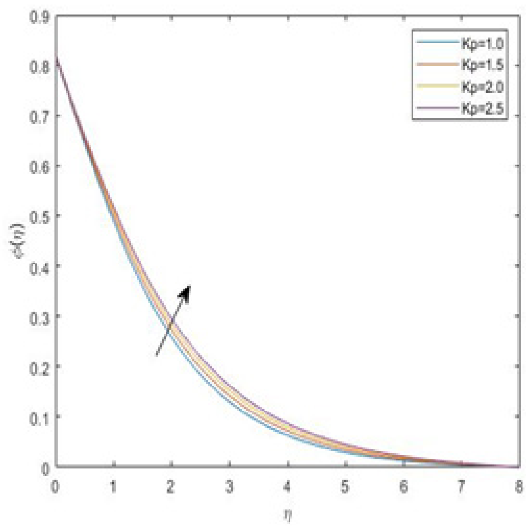

Figure 11. Concentration on *diverse* of K_p.

Table 1. Values of C_{fx}, Nu and Sh

	C_{fx}	Nu	Sh
M = 1.0	-1.9251	2.0193	0.3694
M = 1.5	-2.1237	1.9094	0.3640
M = 2.0	-2.2972	1.8105	0.3598
M = 2.5	-2.4518	1.7204	0.3566
$\beta = 1.0$	-1.3188	2.1424	0.3608
$\beta = 1.5$	-1.1767	2.1376	0.3534
$\beta = 2.0$	-1.1009	2.1334	0.3492
$\beta = 2.5$	-1.0536	2.1300	0.3464
$K_p = 1.0$	-2.1617	1.9066	0.3644
$K_p = 1.5$	-2.3353	1.8073	0.3602
$K_p = 2.0$	-2.4896	1.7169	0.3569
$K_p = 2.5$	-2.6289	1.6338	0.3542

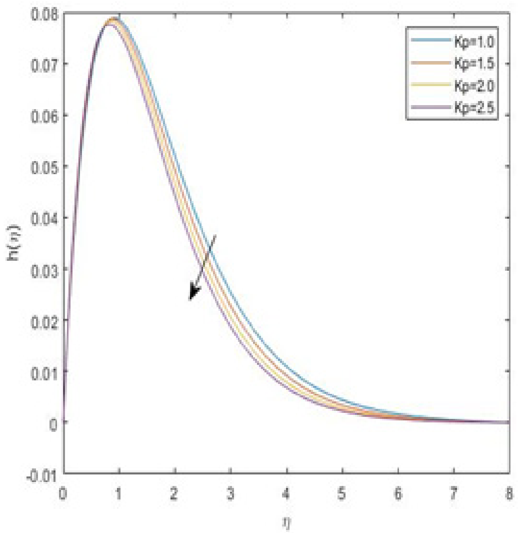

Figure 12. Angular velocity on diverse of Kp.

The fallout of friction drag, Nusselt and Sherwood numeral for distinct of the momentum, casson parameter and porosity are shown in table. The Nusselt and Sherwood numeral retarded by increment of the momentum, casson parameter and porosity (M, β, Kp). Conversely, while Skin friction rises by gain of casson parameter whereas drops by M,Kp.

4.0 Conclusions

In this research numerical solution for the outcome of micro polar casson nano fluid with Porous medium are explored. MATLAB Bvp4c is used to solve the ODEs. The impact of planted variables on the disposal of mass, heat, porous medium and velocity functions is depicted graphically. The major findings are

- The Magnetic parameter, Casson parameter and Porous medium parameter are increased in temperature and concentration profile.
- Table 1 granted Nusselt and Sherwood numbers reduce by increasing the magnetic effect.
- The Velocity profile and Angular velocity profile decreases with enhancement in M, and K_p.

5.0 References

1. Bala Anki Reddy P. Magneto hydrodynamic flow of a Casson fluid over an exponentially inclined permeale stretching surface with thermal radiation and chemical reaction. Ain Shams Eng. J. 2016 June; 7:593-602. https://doi.org/10.1016/j.asej.2015.12.010.
2. Basavaraj K, Elangovan K, Shankar S. Optimization of AL_2O_3 Concentration in Water Based Nano Fluid to Enhance the Heat Transfer for Solar Application. JMMF. 2022 Jul. 12; 70(3A):92-7. https://www.informaticsjournals.com/index.php/jmmf/article/view/30674.
3. Deivanayaki M, Dr. Hemamalini PT. Magneto hydrodynamic Rayleigh Problem with Hall Effect and Rotation. Int. J. Eng. Res. Technol. 2013 Dec.; 2(12):3042-6. https://doi.org/10.17577/IJERTV2IS120846.
4. Mabood F, Das K. Outlining the impact of melting on MHD Casson fluid flow past a stretching sheet in a porous medium with radiation. Heliyon. 2019 Feb; e01216. https://doi.org/10.1016/j.heliyon.2019.e01216.
5. Hemamalini PT, Deivanayaki M. Viscous Dissipation and Heat Transfer Effects in Mhd Rayleigh Problem. Int J Adv Res. 2017 Feb.; 5(2):1314-20. https://doi.org/10.21474/IJAR01/3285.
6. Oyelakin IS, Mondal S, Sibanda P. Unsteady Casson nanofluid flow over a stretching sheet with thermal radiation, convective and slip boundary conditions. Alexandria Engineering Journal. 2016; 55:1025–35. https://doi.org/10.1016/j.aej.2016.03.003.
7. Ullah I, Shafie S, Khan I, Hsiao KL. Brownian diffusion and thermophoresis mechanisms in Casson fluid over a moving wedge. Results in Physics. 2018 Jun; 9:183–94. https://doi.org/10.1016/j.rinp.2018.02.021.
8. Kamran A, Hussain S, Sagheer M, Akmal N. A numerical study of magneto hydrodynamics flow in Casson nanofluid combined with Joule heating and slip boundary conditions. Results in Physics. 2017; 7:3037–48. https://doi.org/10.1016/j.rinp.2017.08.004.
9. Kataria HR, Patel HR. Soret and heat generation effects on MHD Casson fluid flow past an oscillating vertical plate embedded through porous medium. Alexandria Engineering Journal. 2016 Sept.; 55:2125–37. https://doi.org/10.1016/j.aej.2016.06.024.
10. Anwar MI, Rafique K, Misiran M, Shehzad SA. Numerical study of hydrodynamic flow of a Casson nanomaterial past an inclined sheet under porous medium. Heat Transfer Asian Res. 2019 March; pp. 1–28. Wiley Periodicals, Inc. wileyonlinelibrary.com/journal/htj.
11. Thomas NM, Mathew S, Maruthamanikandan S. Effect of Time-Dependent Sinusoidal Boundary Temperatures on the Onset of Ferro convection in a Porous Medium. Journal of Mines, Metals and

Fuels. 2022; 70(3A):78–83. https://doi.org/10.18311/jmmf/2022/30672

12. Venkata Ramudu AC, Anantha Kumar K, Sugunamma V, Sandeep N. Impact of Soret and Dufour on MHD Casson fuid fow past a stretching surface with convective–difusive conditions. Journal of Thermal Analysis and Calorimetry. 2022; 147:2653–63. https://doi.org/10.1007/s10973-021-10569-w.

Nomenclature

(u,v)	Velocity components
β_T	Thermal coefficient
β_c	Concentration coefficient
T	Fluid temperature
T_∞	Uniform temperature
C	Concentration fluid
C_∞	Uniform concentration
α	Angle of inclination
σ	Electric conductivity fluid
B_0	Uniform magnetic field
g	Gravitational acceleration
K_1	Permeability of the fluid
q'''	Irregular heat parameter
D_m	Mass diffusivity
C_s	Concentration susceptibility
K_T	Thermal diffusion ratio
T_m	Mean temperature
B_{iT}	Thermal Biot Number
B_{ic}	Mass Biot Number
ɤ	Velocity slip parameter
G_{rT}	Thermal Grashot number
G_{rc}	Solutal Grashot number
M	Hartmann number
N_r	Non-linear radiative parameter
S_r	Soret number
S_C	Schmidt number
D_u	Dufour number
E_c	Eckert number
K_r	Chemical parameter
q_r	Radiative heat
K	Non dimensional parameter
P_r	Prandtl number